Radiated seismic energy from coda measurements and no scaling in apparent stress with seismic moment

Annemarie Baltay,[1] German Prieto,[1,2] and Gregory C. Beroza[1]

Received 30 June 2009; revised 11 March 2010; accepted 9 April 2010; published 31 August 2010.

[1] The seismic coda consists of scattered waves that leave the earthquake source in a variety of directions. The averaging of source radiation that results leads to stable ground motion spectra that we use as the basis for a robust measurement of radiated wave energy. We apply an empirical Green's function (EGF) method to the seismic coda in order to investigate scaling of the radiated seismic energy. We correct for path effects in the spectra of earthquakes by using a stack of closely located, small earthquakes as an EGF. We apply this approach to four earthquake sequences in western North America that span a magnitude range from M_w 3.0–M_w 7.1. Our estimates of scaled energy are consistent with independent measurements, where available. We find no dependence in individual seismic energy estimates on source-station distance, which validates the EGF approximation. We find that a constant scaled energy of 3.5×10^{-5} provides a reasonable fit to the data, with no dependence of the scaled energy on seismic moment.

Citation: Baltay, A., G. Prieto, and G. C. Beroza (2010), Radiated seismic energy from coda measurements and no scaling in apparent stress with seismic moment, *J. Geophys. Res.*, *115*, B08314, doi:10.1029/2009JB006736.

1. Introduction

[2] A long-standing discrepancy exists in studies of radiated seismic energy. Some studies find that the scaled energy, the ratio of seismic energy to seismic moment, varies systematically with earthquake size [e.g., *Kanamori et al.*, 1993; *Abercrombie*, 1995; *Mayeda and Walter*, 1996; *Mori et al.*, 2003; *Walter et al.*, 2006], while others find that it does not [e.g., *Choy and Boatwright*, 1995; *Ide and Beroza*, 2001; *Prieto et al.*, 2004; *Yamada et al.*, 2007]. The scaling of seismic energy is an important issue for both the physics of earthquake faulting and for strong ground motion prediction. For earthquake physics, a break in scaling might be diagnostic of a characteristic length or time scale in the faulting process. For strong ground motion prediction, if large earthquakes radiate seismic energy more efficiently than do small earthquakes, then they have the potential to generate more intense, strong ground motion.

[3] The controversy in energy scaling arises because, even though radiated energy is a scalar quantity, it is difficult to measure accurately. Seismic waves are generated with strong angular variations at the source due to both the radiation pattern and source directivity. As these waves propagate, they attenuate, scatter, and focus/defocus, and they are subject to strong frequency-dependent site effects in the near surface. All of these factors influence wave amplitude and, because they are difficult to correct for accurately, independent studies of the same earthquake may find seismic energies that differ by an order of magnitude [*Singh and Ordaz*, 1994].

[4] Many sources of variability exist between different studies [*Ide et al.*, 2003], and it is difficult to consistently correct for wave propagation effects over many orders of magnitude and across different tectonic settings. Some studies have found no evidence that scaled energy increases with seismic moment. *Ide and Beroza* [2001] compiled previous studies, applied adjustments that would correct for probable bias in measurements of the radiated energy, and found that although scaled energy varies widely for a given earthquake size, it does not show a systematic trend with seismic moment. *Prieto et al.* [2004] used spectral stacking and came to a similar conclusion for small earthquakes. *Imanishi and Ellsworth* [2006] found constant scaled energy for even smaller earthquakes.

[5] Other studies have come to the opposite conclusion, finding that scaled energy increases systematically with increasing seismic moment. *Mori et al.* [2003] found an increase in scaled energy with moment for aftershocks of the 1994 Northridge earthquake. *Takahashi et al.* [2005] found an even stronger scaling, with scaled energy increasing as $M_o^{0.44}$ for earthquakes in Japan. Perhaps the strongest evidence for dependence of the scaled energy on seismic moment comes from energy estimates based on the scattered waves of the seismic coda.

[6] *Mayeda* [1993], *Mayeda and Walter* [1996], and *Mayeda et al.* [2003] have developed a method to isolate the coda source spectra by empirically correcting for path and site effects. In this method, narrowband envelopes of the coda are created. Then, the decay shape of the coda envelope with time is modeled as $t^{-\gamma} \exp(-bt)$, and the parameters b and γ are parameterized with distance. Empirical envelopes are created

[1]Department of Geophysics, Stanford University, Stanford, California, USA.
[2]Now at Physics Department, Universidad de los Andes, Bogotá, Colombia.

0148-0227/10/2009JB006736

with the parameters and are fit again to the data. The coda spectral amplitude is determined as the linear term in the fit of the synthetic envelopes to the observed envelopes. *Mayeda and Walter* [1996] used an empirical Green's function (EGF) correction technique to estimate the scaled energy, and they concluded that it increases as $M_o^{0.25}$, which represents a very strong trend. *Mayeda et al.* [2005] found scaling with an exponential slope of 0.12 to 0.38 for four distinct geographical areas. In addition, *Mayeda et al* [2007] extended their empirically derived coda spectra to a spectral ratio method, and they found that spectra were not self-similar. Until these disparate conclusions are reconciled, the question of whether scaled seismic energy varies systematically with seismic moment must be considered unresolved.

[7] In this study, we measure seismic energy using the scattered waves of the seismic coda without empirically fitting the envelope decay shapes. A distinct advantage of coda waves is that, because they are scattered, they average factors such as directivity and a radiation pattern to give a more stable amplitude measurement [*Mayeda*, 1993; *Mayeda et al.*, 2007]. A major benefit of this method lies in the simplicity behind it. Without having to make the envelope shape corrections, we make many fewer assumptions in the analysis. We compare the coda for different earthquakes recorded at the same station using what amounts to an empirical Green's function technique to remove sources of common-mode error, primarily propagation effects, from the measurement. The result is a stable measure of relative wave amplitudes over a wide frequency range that can be used to estimate the radiated energy. We apply this technique to four earthquake sequences in western North America that, taken together, span a magnitude range of $3 \leq M_w \leq 7.1$. Our results agree with other energy estimates for the larger earthquakes in our sample, and we find that scaled energy does not increase with seismic moment for this data set. Examination of a larger earthquake catalog will determine whether this result generalizes.

2. Empirical Green's Function Approach for Coda Spectral Amplitude

[8] Waves generated by an earthquake attenuate, focus/defocus, and scatter as they propagate through the complex geology of the Earth. The seismograms that result are a mixture of source and propagation effects. The empirical Green's function approach assumes that the predominant differences for earthquakes located close to one another arise from source effects [*Mueller*, 1985]. We use this principle to isolate source effects and, in particular, to examine the relative energy radiation of closely spaced events.

[9] We first assume that a small event has an ideal Brune spectral shape, obeying

$$u(f) = \frac{\Omega_o}{1 + (f/f_c)^2} \tag{1}$$

where *u(f)* is the far-field displacement spectra; Ω_o is the long period amplitude level, proportional to seismic moment; and f_c is the corner frequency [*Aki*, 1967; *Brune*, 1970]. The use of a different ω^{-2} model [*Boatwright*, 1978] yields no effect on the scaled energy but, because of a sharper corner frequency, the Boatwright model shifts all the energy estimates ~13% higher relative to the Brune model. Next, we assume that this small event, typically $M_w \sim 3$, has a short duration, and hence a high corner frequency near 8–10 Hz, below which the EGF can be considered to approximate the point source response. The EGF can then be used to extract the spectral source characteristics of the larger events at frequencies below the EGF corner frequency. When using direct waves or individual events, stable results depend strongly on the choice of the Green's function event. Because we use the spectra of the seismic coda and an average of many smaller events as our EGF, our estimate is less dependent on the choice of EGF than other methods.

[10] We filter the displacement records with a two-pass four-pole Butterworth filter in narrow bands between 0.01 Hz and just less than the Nyquist frequency of the instruments (10 Hz for Hector Mine and Parkfield and 20 Hz in the case of Cerro Prieto and Wells) (Figure 1a). As well, 20 Hz is about the limit of useful data possible from surface stations in southern California and the western United States. Any effect that the antialias filter might have as an amplitude as the Nyquist frequency is approached affects each event by proportionally the same amount, such that it is eliminated when working with relative spectral amplitudes. We then take the envelope as the distance between the filtered record and its Hilbert transform:

$$E(t,f) = \sqrt{u(t)^2 + h(t)^2} \tag{2}$$

Data and envelopes are visually checked to ensure that there are no clipped records, dropouts, spikes, or aftershocks in the coda. In some cases, we use the accelerometer data in place of the broadband for the large events at close distances. The

Figure 1. (a) Broadband coda seismogram and narrowband envelopes for three representative events at one station are shown for two/three schematic narrow passbands. Empirically derived starting and ending points of the envelope amplitude measurements are shown with stars. (b) Coda amplitude values at each frequency are found from the average of the narrowband envelope over the windows i–viii between stars. Representative frequency bands are indicated by numerals i–viii; other frequencies not shown in (a) indicated by open circles. Other events shown in gray; coda amplitudes found in the same manner as for the other events. (c) Displacement source spectra created by fitting the M_w 3.0 EGF event to an ideal Brune shape after calculating its corner frequency. Larger events are adjusted by flattening the leftmost point of each next larger event and propagating the correction upward. Finally, spectra are adjusted up on a log scale to match the moments while preserving spectral ratios. (d) Multiplication by ω yields velocity source spectra. Spectra are extrapolated to high and low frequencies. Energy is calculated from the integral of the moment-rate spectra. An ω^{-2} decay in displacement spectra, ω^{-1} in velocity, is assumed for all events for frequencies greater than our measurement window, and this follows the asymptotic shape of the larger events nicely. However, for the smallest events, the spectra has not yet reached that decay shape, so the ω^{-2} decay is conservatively underestimating the spectra, which may actually lead to underestimation of the energy in the smaller events.

coda spectra are then created from a window in time over the length of the coda envelope (Figure 1a).

[11] The coda window starts just after the *S*-wave arrival. We vary the window lengths with frequency in order to maximize the duration of the useful signal, but we avoid a possible bias for large versus small events by keeping window lengths constant across magnitude. The coda envelope reaches the noise threshold sooner for smaller events, such that the maximum length for the smallest event considered at each station sets the window length for all of the events.

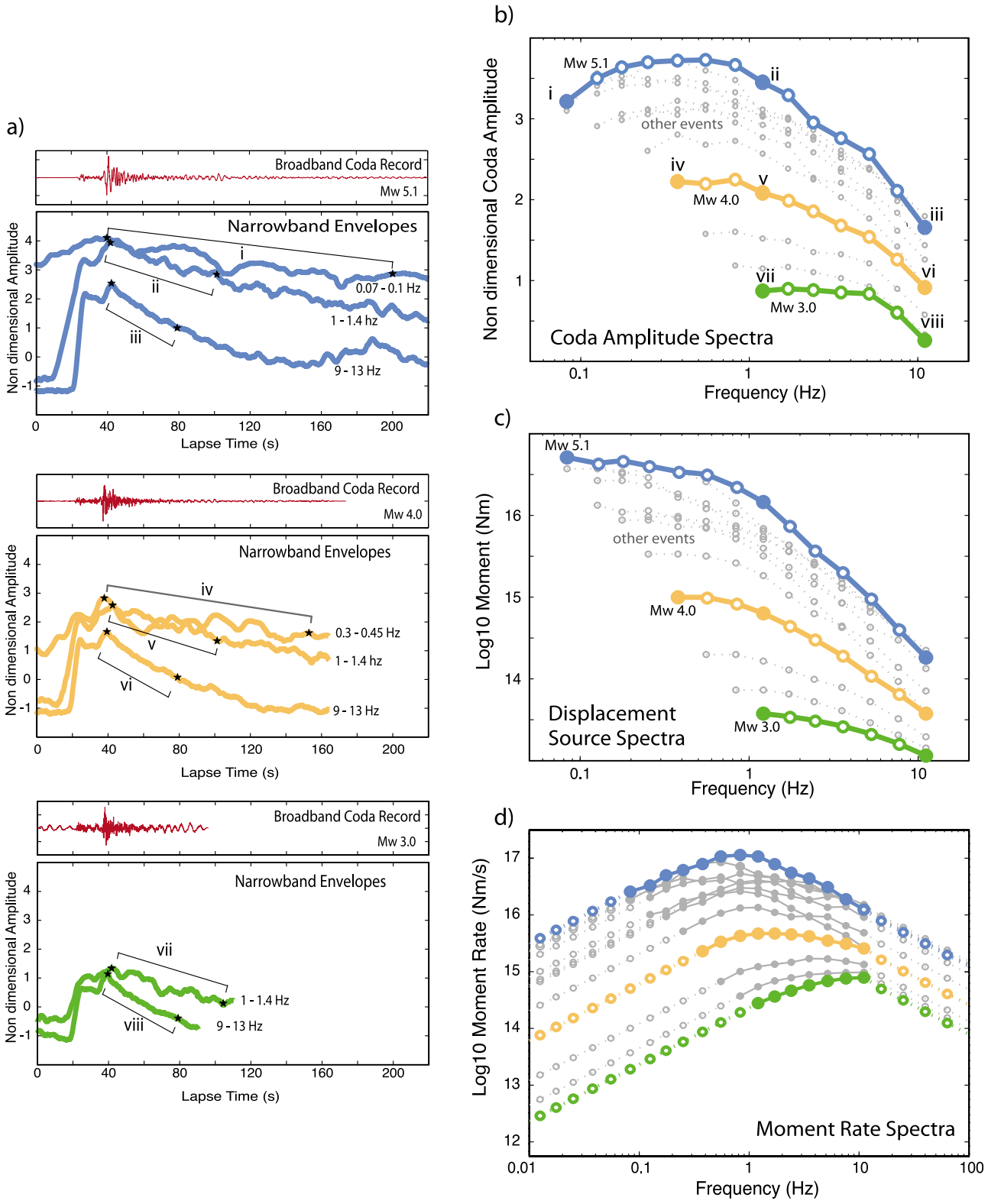

Figure 1

Table 1. Function of Assumed Stress Drop on the Scaling Exponent

Hector Mine						
Assumed for smallest event			Derived			
*Stress Drop (MPa)	*Corner Frequency (Hz)	*Duration (s)	Scaling Exponent	95% Conf. Interval	STD	ε
1	4.80	0.21	0.265	0.07	0.29	1.080
3	6.93	0.14	0.091	0.08	0.22	0.300
5	8.21	0.13	0.075	0.08	0.23	0.242
10	10.35	0.10	0.058	0.09	0.23	0.185
	magnitude 3.1 event					
Parkfield						
Assumed for smallest event			Derived			
*Stress Drop (MPa)	*Corner Frequency (Hz)	*Duration (s)	Scaling Exponent	95% Conf. Interval	STD	ε
1	4.50	0.22	0.073	0.09	0.16	0.236
3	6.48	0.15	0.001	0.09	0.16	0.004
5	7.68	0.13	−0.025	0.09	0.16	−0.073
10	9.68	0.10	−0.053	0.09	0.16	−0.150
	*magnitude 3.2 event					
Cerro Prieto						
Assumed for smallest event			Derived			
*Stress Drop (MPa)	*Corner Frequency (Hz)	*Duration (s)	Scaling Exponent	95% Conf. Interval	STD	ε
1	4.95	0.20	0.088	0.08	0.14	0.287
3	7.13	0.14	0.016	0.09	0.15	0.049
5	8.46	0.12	−0.010	0.09	0.16	−0.029
10	10.66	0.09	−0.037	0.10	0.17	−0.108
	*magnitude 3.1 event					
Wells						
Assumed for smallest event			Derived			
*Stress Drop (MPa)	*Corner Frequency (Hz)	*Duration (s)	Scaling Exponent	95% Conf. Interval	STD	ε
1	6.30	0.16	0.080	0.10	0.18	0.259
3	9.08	0.10	0.022	0.10	0.19	0.068
5	10.77	0.09	−0.001	0.10	0.19	−0.003
10	13.57	0.07	−0.027	0.10	0.20	−0.080
	*magnitude 2.9 event					

The stress drop is assumed in each case, and the corner frequency and duration are calculated for the smallest EGF event according to equation (3) and the relationship of duration as the inverse of the corner frequency. The scaling exponent is found from the best fit line to the scaled energy from the stacked spectra across all stations. A 95% confidence interval is from the fit, and the standard deviation describes the residuals. The scaling parameter ε [after *Kanamori and Rivera*, 2004] describes the deviation from no scaling, so that a value of $\varepsilon = 0$ represents self-similarity. In contrast, *Mayeda et al.* [2003] have found a scaling exponent of 0.25 and $\varepsilon = 1$. The scaling exponent is equal to $\varepsilon/(\varepsilon+3)$. The shaded areas indicate stress drops, corner frequencies, and durations that are unreasonable for the small earthquake.

Because we use smaller events, our method is limited to shorter window lengths for the larger events than are often used in other coda studies [e.g., *Mayeda and Walter*, 1996]. Shorter window lengths may increase the interstation variability and reduce the stability of the coda. We compensate for any loss in variance by including many stations in each analysis, up to 10 times as many as in previous coda studies. Coda envelope durations are measured empirically over magnitudes, frequencies, and station-event distances, and the model is applied to all observed events within each sequence. The coda spectra value at each frequency is the time average of the narrow-band window for each frequency (Figure 1b). Once we measure the coda spectra, we stack events by magnitude. We stack events below magnitude 4.5 into bins that span approximately 0.25 magnitude units.

[12] Source spectra are isolated using a stack of several small events ($3 < M < 3.25$) as an empirical Green's function. The EGF is assumed to have a short duration and hence a high corner frequency. We estimate its corner frequency assuming a stress drop of $\Delta\sigma = 3$ MPa and the relationship

$$f_o = \left(\frac{\Delta\sigma}{8.5M_o}\right)^{1/3} \tag{3}$$

after *Hanks and Thatcher* [1972]. We tested various choices of stress drop, ranging from 0.10 to 10 MPa, and found that the scaled energy is dependent on this initial choice of stress drop. A very small stress drop implies a very low corner frequency, causing the smaller events to have proportionally less energy. As the assumed stress drop increases, the scaling exponent decreases (Table 1). We use a stress drop of 3 MPa in our analysis, as that is in the middle of the most commonly reported values for ~M_w 3 events [*Kanamori and Anderson*, 1975; *Abercrombie*, 1995; *Shearer et al.*, 2006; *Allmann*

and *Shearer*, 2009]. The EGF in each case has a corner frequency between 6.5 and 9 Hz and asymptotically approaches a flat spectrum at low frequencies and a decay of ω^{-2} at high frequencies, so it is not exactly flat in our instrument bandwidth, especially near the corner frequency.

[13] The EGF is fit to an ideal Brune spectral model over the frequency band we work in, and all the larger events are adjusted accordingly, to correct for propagation effects. Spectra of larger events are adjusted so that the observed spectral ratio between the EGF and the larger events is maintained at all frequencies. Because of the limited signal-to-noise ratio of the smaller events, we can't do this over the entire range of frequencies. Each time we use a larger event, we flatten the lowest spectral measurement to match the second lowest measurement, and we adjust all larger events proportionally. We proceed in a stepwise manner with events of increasing seismic moment until all measurements have been adjusted. Finally, the spectra are shifted such that the long period end of the spectra fit their seismic moment by assuming a moment only for the largest event and allowing all the smaller events to follow (Figures 1b and 1c). Once displacement source spectra are determined for all events and stations, the spectra of all events at each station are adjusted in what amounts to a station correction for amplitude to best fit the stacked spectra across all stations. In this process, the relative spectral amplitudes for all earthquakes as recorded at each station are always preserved.

[14] Radiated energy is calculated from the integral of the velocity spectrum, ω. $M(\omega)$, where ω is the angular frequency and $M(\omega)$ is the moment-rate spectrum. To estimate the energy, spectra should be integrated over all possible frequencies; however, the 40 samples per second sampling rate for many of the stations limits our analysis to a Nyquist frequency of 20 Hz. For some of the earthquakes, a significant fraction of the energy will be radiated at higher frequencies. Thus, the moment-rate spectra are extrapolated to both the upper, and lower, frequency limits. Following the ω^{-2} decay of the displacement spectra, we model the velocity spectra to decay as ω^{-1} above the corner and ω^{1} below (Figure 1d). Finally, energy is estimated from the area under the square of the velocity spectra, using the constants ρ, the material density as 2700 kg/m^3, and β as the S-wave velocity, 3.5 km/s [e.g., *Mayeda and Walter*, 1996].

$$E_R = \frac{1}{4\pi^2\rho\beta^5}\int_0^\infty \left|\omega \cdot M(\omega)\right|^2 d\omega \tag{4}$$

[15] We examine the effect of limited bandwidth on energy estimation in our data, as over 80% of the seismic energy may be radiated at frequencies greater than the corner frequency [*Ide and Beroza*, 2001]. The cumulative fractional energy indicates the proportion of energy measured as a function of frequency (Figure 2). In the Brune model, it can be seen that about 20% of the energy is measured below the corner frequency, which is near the instrument bandwidth for very small events. Our data indicates as little as 55% of the energy is in the instrumentally measured bandwidth for our smallest events, near Mw ~3. Even for intermediate-size events, a substantial fraction of the radiated energy is not measureable directly. Lacking data recorded to higher frequencies, this is an unavoidable consequence of the broadband character of the radiated energy. Some extrapolation to higher frequencies is required. The shapes of the cumulative energy function for the events we analyze are similar to the ideal model. The Hector Mine mainshock, however, was a complex rupture with a duration of over 10 s, occurring on a branching fault system; thus, we do not expect it to follow the ideal Brune shape.

3. Four Study Areas

[16] The method requires earthquakes close enough together that they share common path effects [e.g., *Hough*, 1997]. We analyze four earthquake sequences from western North America: the M_w 7.1 1999 Hector Mine sequence; the M_w 6.0 2004 Parkfield earthquake sequence; the 2008 swarm near the Cerro Prieto geothermal field in Mexico, with several events of M_w 5; and the M_w 6.0 2008 Wells, Nevada sequence (Figure 3). In each case, the moment magnitudes are determined from the global centroid moment tensor catalog for larger events and the National Earthquake Information Center (NEIC) catalogs for the smaller event. These four data sets include events with both a range of magnitude over which moment-dependent energy scaling has been observed previously and a diversity of mechanisms. For each sequence, at least 40 events occur in close proximity to one another, and they are well recorded on broadband seismic networks. The Hector Mine mainshock and aftershocks are the most spatially distributed due to the long and complex rupture, but about 80% of the events are within 25 km of the average location and, with the exception of the closest station (HEC in Hector, CA, run by the Caltech Regional Seismic Network), the nearest stations are 80 km away. At Parkfield, the events are again distributed along the fault trace, with 80% within 10 km of the average location and, with the exception of one close station at Parkfield, the stations are at least 50 km away. The Wells events are the most tightly clustered, with 90% within 10 km of each other and, in Cerro Prieto, 85% are within 20 km from the average location. We analyze $M_w >$ 4 earthquakes individually and groups of smaller events in a stacked aggregate, the smallest of which is used as the EGF [*Prieto et al.*, 2004]. We believe that these distances are adequate to use in the EGF method, given that we stack many smaller events to create the EGF, and because we use the more stable coda in the spectra. At close stations for the large events, instrument-response-corrected low-gain recordings are used, while for smaller events and at larger distances, instrument-response-corrected broadband high-gain recordings are used. We repeat the analysis at approximately 30 stations for each earthquake sequence, at distances ranging from several kilometers to 250 km. The large number of stations reduces the variability in the averaged measurements.

4. Scaled Energy Versus Moment

[17] In total, we analyzed 225 events spanning a magnitude range from M_w 2.8 to M_w 7.1. Once we stack over the smaller magnitude bins, we have estimates of radiated energy for 53 events. The tectonic settings vary from right-lateral strike slip on the San Andreas to normal faulting in the basin and the range province (NEIC moment tensor solutions, http://neic.usgs.gov/). We find that the apparent stress, defined as

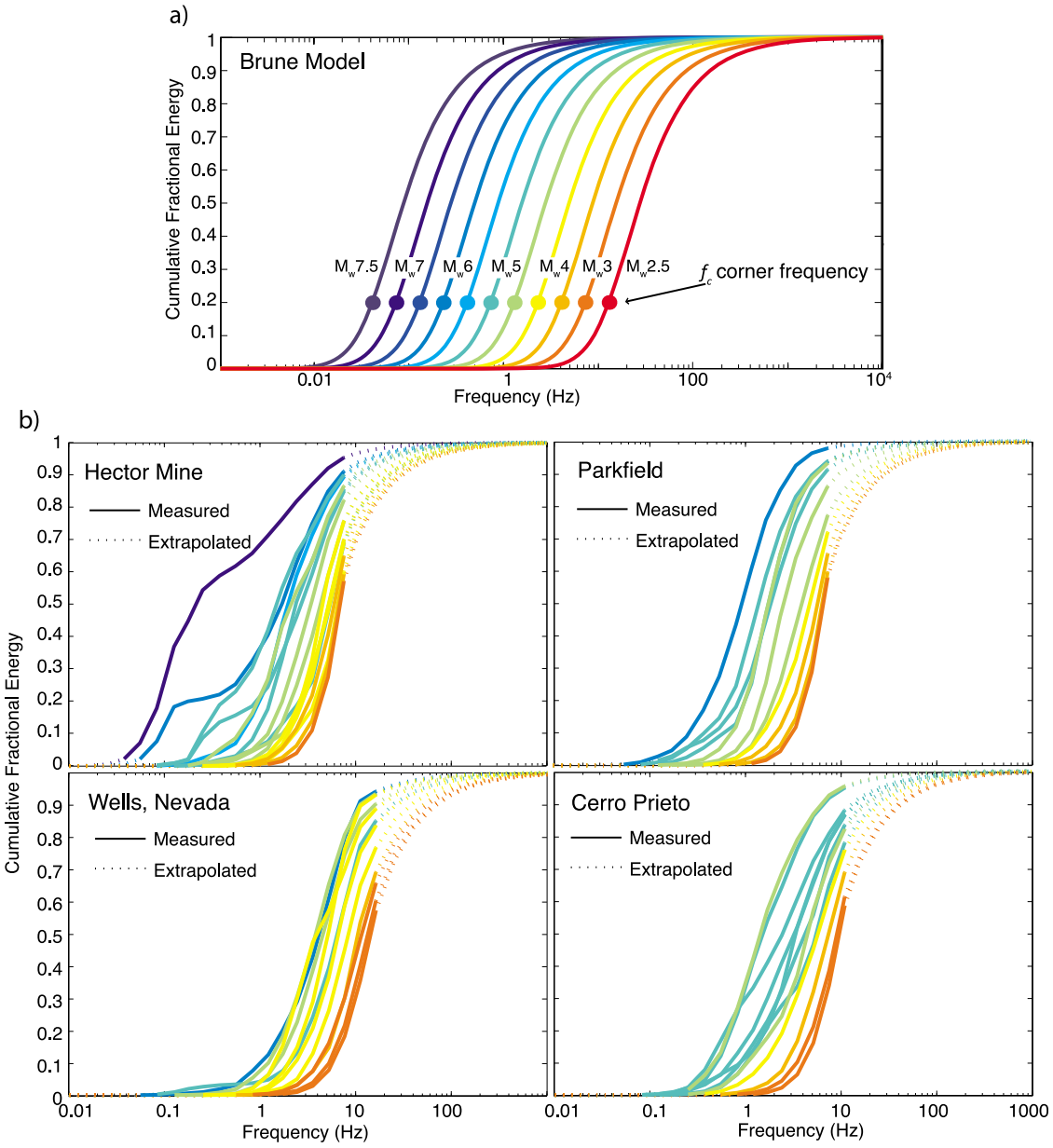

Figure 2. Cumulative fractional energy with frequency. (a) Ideal Brune ω^{-2} models for a range of magnitudes. Energy measured up to the corner frequency represents only 20% of the total energy. (b) Cumulative energy for all of the events in the four study areas. Colors of the data cumulative energy indicate the magnitude as shown in the Brune model in Figure 2a. Solid lines indicate the measurement range, while dashed lines indicate the extrapolated portion of the energy estimate, analogous to the dotted lines in Figure 1d. For some of the smallest events, only 55% of the energy is contained in the instrument bandwidth, implying that extrapolation into higher frequencies is required to completely measure the radiated energy.

$$\tau_a = \mu \frac{E_R}{M_o} \tag{5}$$

with shear modulus μ [*Wyss*, 1970], for the four earthquake sequences we studied varies between about 0.2 and 3 MPa, but it shows no dependence on seismic moment (Figures 4 and 5).

[18] The range of interstation measurements can be seen in Figure 4 as dots, and the measurements are represented statistically in Figure 5 with box plots. Box and whisker plots compactly and nonparametrically display the dispersion in data. The middle bar is the median; the top and bottom of the box indicate the 25th and 75th percentiles, the difference of which is the interquartile range; whiskers show the distance to the farthest data point within the interquartile range; and pluses are outlying data points, defined as farther than 1.5 times the interquartile range. The individual measurements are closely clustered, with few outliers, and interquartile ranges are small. Best fit lines to the stacked spectra are

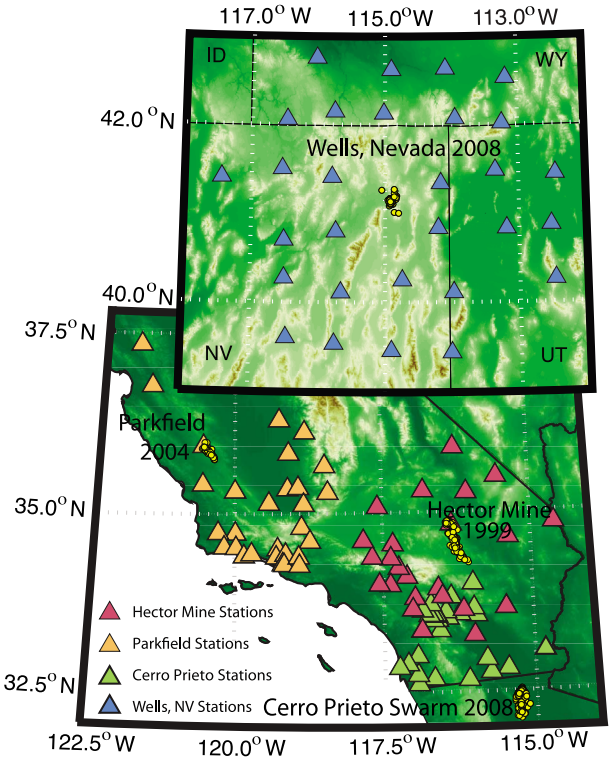

Figure 3. Study areas and stations used in analysis.

shown in Figure 5, as well as the 95% confidence interval on the fits.

[19] The Hector Mine mainshock and its aftershocks have apparent stress around 1.0 MPa. We find that the energy of the M_w 7.1 Hector Mine mainshock is 6.1×10^{15} J, which is within half an order of magnitude to two independent studies that find the energy to be 3×10^{15} J [*Venkataraman et al.*, 2002] and 3.4×10^{15} J [*Boatwright et al.*, 2002], as well as the published NEIC radiated energy of 1.9×10^{15} J (http://neic.usgs.gov/). These estimates fall within the interstation scatter for this earthquake. The average E_R/M_o ratio is 4.1×10^{-5} for this sequence, or an apparent stress of 1.1 MPa. Our least squares fit to the data is $E_R/M_o \sim M_o^{0.091+/-0.08}$. We analyzed 77 events in the Hector Mine mainshock-aftershock, the smaller of which stack into four magnitude bins between M_w 3.0 and M_w 4.0, for 18 total energy measurements. The mainshock has a near-vertical right-lateral strike-slip mechanism, consistent with the sense of motion in southern California.

[20] The Parkfield events have a slightly higher apparent stress. The interstation scatter for this sequence is low. The average scaled energy is 5.6×10^{-5}, or an apparent stress of 1.8 MPa. The relationship found for the Parkfield subset is $E_R/M_o \sim M_o^{0.001+/-0.09}$, which is consistent with zero slope. We find the energy of the M_w 6.0 mainshock to be 8.1×10^{13} J. This is higher than what was found by *Ma et al.* [2008], who estimated the energy of the mainshock as 1×10^{13} J, but their estimate was based on a dynamic rupture model of

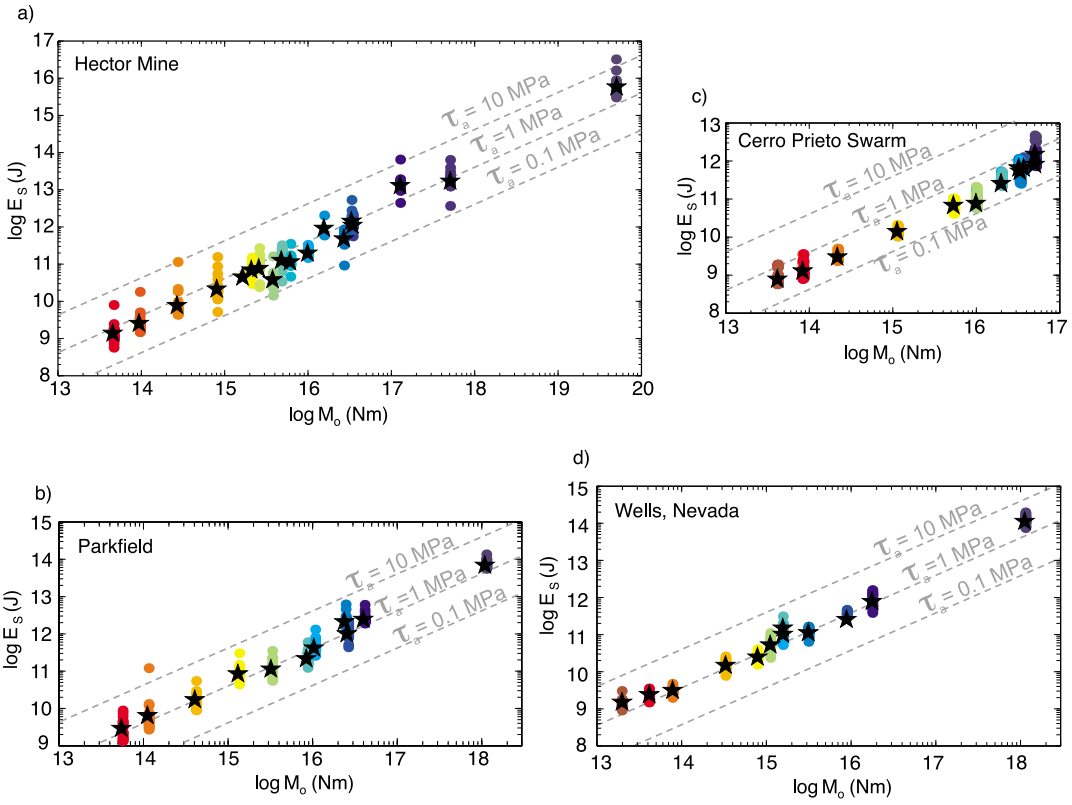

Figure 4. Radiated energy versus moment for the four study areas. Circles show the energy estimates at individual stations for each event. Black stars indicate the mean of the station estimates. Energy estimated from the spectra stacked across stations is not shown explicitly here, as it is within the symbol size of the mean energy shown in stars. Dashed lines show constant apparent stress.

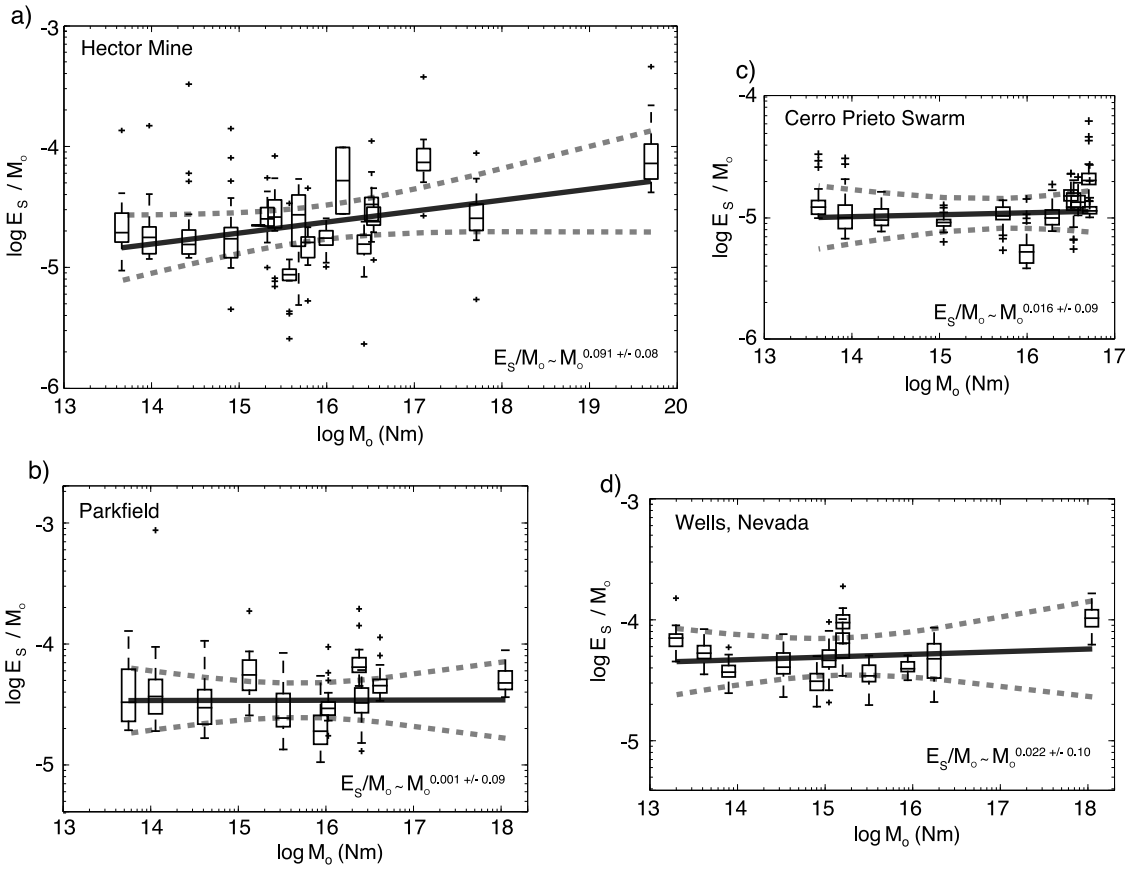

Figure 5. Scaled energy versus moment for the four study areas. Data range given by the box and whisker plot, where the middle bar is the median and the box indicates the 25th and 75th percentiles, the difference of which is the interquartile range. The whiskers show the distance to the farthest data point within the interquartile range and the pluses are outlying data points, defined as more than 1.5 times the interquartile range. For most events, the whiskers are small, and few, if any, outliers exist, showing that the interstation scatter is tight. The heavy black line shows the best fit to the stacked spectra (also shown in Table 1), and the dashed gray lines are the 95% confidence intervals on the fit.

the mainshock, which only provides a lower bound on the radiated energy. Similar to the Hector Mine sequence, the Parkfield mainshock was a nearly pure right-lateral strike slip along the San Andreas fault. The aftershocks numbered 47 and, after the binning of the 39 smallest events, between M_w 2.8 and M_w 4.0, there were 11 final energy estimates.

[21] The Wells, Nevada 2008 sequence has the lowest interstation variability, possibly because of the even azimuthal station spacing and similarity of the USArray instruments. For the M_w 6.0 mainshock, we find an energy of 1.2×10^{14} J, about an order of magnitude higher than the NEIC estimate of 8.9×10^{12} J. The average E_R/M_o ratio is 5.7×10^{-5}, which corresponds to an apparent stress of 1.8 MPa. The least squares fit to the data is $E_R/M_o \sim M_o^{0.022+/-0.10}$. The Wells, Nevada, M_w 6.0 mainshock occurred in a normal faulting regime, consistent with the active tectonics of the basin and the range. We included 56 events within the aftershock sequence, which we binned to yield 12 radiated energy estimates.

[22] The earthquakes in the Cerro Prieto sequence also have low interstation scatter. Here again, the apparent stress for all of the events falls between 0.1 and 1 MPa, and the average scaled energy is 1.7×10^{-5}, which corresponds to an apparent stress of 0.55 MPa, the lowest of all of the sequences. This lower apparent stress may be explained by a difference in the actual shear wave velocity β or, possibly, material density ρ in the Cerro Prieto area. We hold β constant between study areas, yet the Cerro Prieto area is composed of softer sediments, which may warrant a smaller β value. There is no obvious trend of increasing apparent stress with increasing moment. We found the relationship $E_R/M_o \sim M_o^{0.016+/-0.09}$ for the best fit to the Cerro Prieto data. Forty-three total events in the sequence are analyzed, from M_w 2.8 to M_w 5.1, with several events in the M_w 5 range. The 35 smallest events are binned into four small-magnitude bins, resulting in 12 total estimates. The Cerro Prieto earthquakes have oblique normal/right-lateral strike-slip motion, and they occur near the Cerro Prieto geothermal field on the west side of a step over on the southern end of the San Andreas fault system, an area of both extension and right-lateral movement.

[23] Taken altogether, our results are consistent with each other (Figure 6a) and with scaled energy from events that have been analyzed previously by other methods (Figure 6b), which supports the reliability of our empirical Green's function method. Our energy estimates indicate constant E_R/M_o, with an average scaled energy for all events of

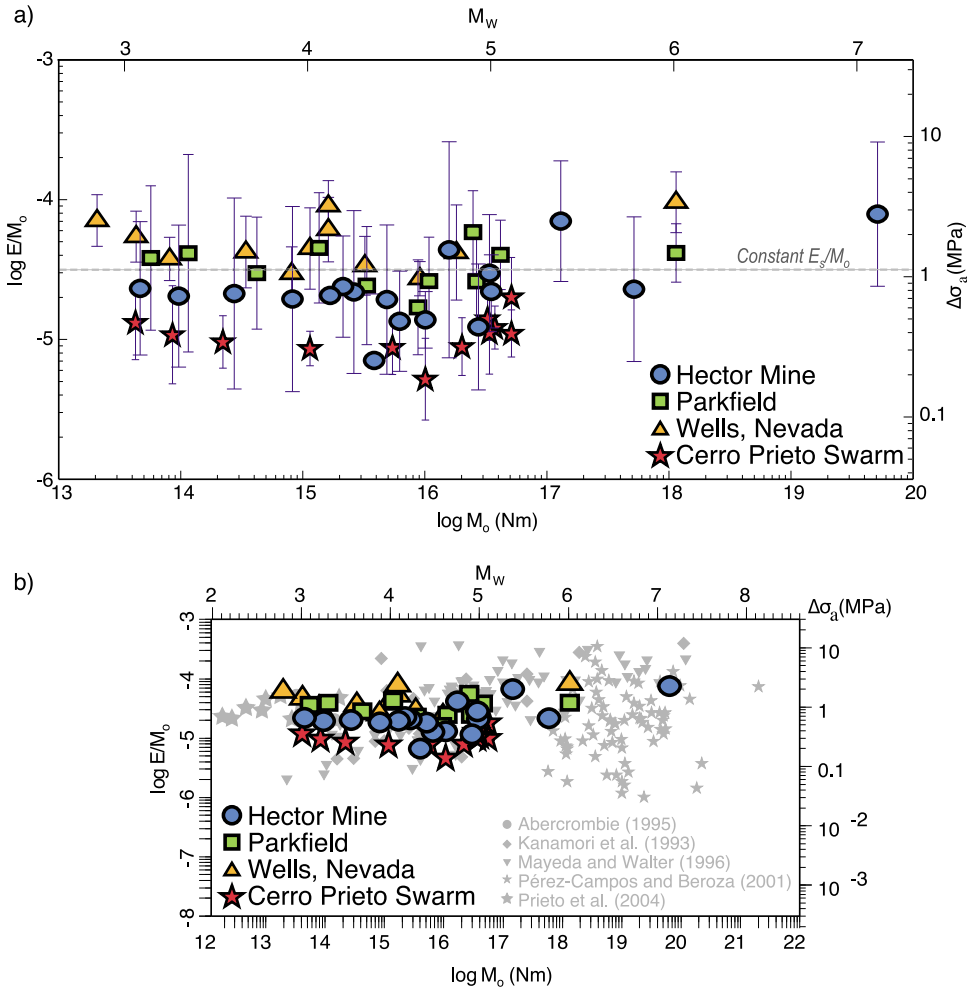

Figure 6. Scaled energy for all four data sets. (a) Large symbols show mean value of scaled energy for each location and event. Gray error bars show 5 and 95% intervals on the interstation scatter. (b) Large dark symbols indicate the average scaled energy for each data set overlain on *Ide and Beroza* [2001]. Estimates from this study agree well with the previous results.

$\sim 3.5 \times 10^{-5}$, which corresponds to an apparent stress of 1.2 MPa. We do not have enough events to fit to a nonlinear or stepwise shape. The best fit to our observations includes the case of no scaling of scaled energy with seismic moment; that is, $E_R/M_o \sim M_o^0$. We find an ε, as defined by *Kanamori and Rivera* [2004], close to 0, indicating self-similarity (Table 1).

5. Validation of Empirical Green's Function Assumptions

[24] We assume that for each seismic station, propagation effects are common to each earthquake in a sequence, such that spectral ratios are controlled by source effects. Using this assumption, we estimate the energy for each event at each station from the coda source spectra, and then we stack the spectra across all of the stations. The result is a stable solution, but we can use several aspects of the result and the residuals to confirm that the assumptions that went into our analysis are reasonable.

[25] To test the path assumptions, we examine the energy measurements from stations at varying distances from the events (Figure 7). We find no systematic behavior in the trends of the scaled energy estimates with distance, which indicates the EGF assumption properly accounts for wave propagation effects in the coda at all the distances considered. We also find that the interstation scatter is similar at all distances. Both of these observations support our assumption that the coda spectral ratio measurements reflect source effects.

[26] Another measure of the reliability of our results is the scatter in the estimates at different stations. The scatter in individual station measurements is consistent within an order of magnitude or less for these events. Once we average over stations, the uncertainty is greatly reduced. Furthermore, the station-averaged spectra follow the widely observed ω^{-2} decay at frequencies higher than the corner (Figure 8).

[27] In all cases, we have made several key assumptions. The first is to model the EGF event with a Brune spectrum with an ω^{-2} high-frequency spectral decay and a smooth variation in amplitude near the corner frequency, following equation (1). To find this shape, we use a stress drop of 3 MPa and the M_w from the average magnitude of the stacked smaller events, in equation (3). The amount of scaling found in this

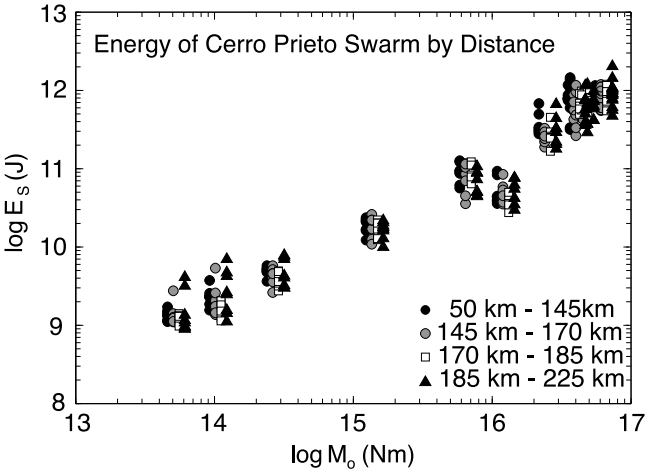

Figure 7. Energy from the Cerro Prieto data compared to station-to-event distance. Different symbols (black circle, gray circle, white square, and black triangle) show energy estimates for increasing station-event distances. The different symbols for each are separated along the moment scale for visual clarity. The estimates show similar scatter and no distance dependence in the method.

analysis is dependent on the initial assumption of stress drop, illustrated in Table 1. If the assumed stress drop used to model the EGF is low, less than 1 MPa, then the scaled energy depends on seismic moment. Likewise, if we assume a very high stress drop, greater than 10 MPa, then we find negative scaling. The choice of 3 MPa is consistent with stress drops found in numerous other studies. Although we assume a shape for the smallest event, the Brune-like behavior for the larger events (Figure 8) is derived from the data, and it is not assumed.

[28] Our second assumption is made while correcting for the path effects after the EGF is modeled. Because the spectrum of the EGF is band limited, we propagate the corrections for each larger spectrum upward. However, we only correct one frequency point for each successively larger event. In each sequence, the smaller events are stacked into four event bins, the smallest of which is modeled as the EGF. The remaining three bins each incur one corrected frequency point in removing the path effects. Another 16 unstacked, larger events over the four sequences each have one corrected frequency point, out of 37 total events. The other large events are corrected by the same amount. Finally, we tie all of the spectra to an absolute moment, using the magnitude of the largest event, which is well known from independent studies. All other events are shifted by the same moment.

6. Conclusion

[29] We use an empirical Green's function method assumption on the seismic coda to estimate seismic energy. We take advantage of the averaging properties of the coda by creating spectra over a coda envelope time window, which is more stable than a single direct measurement. The EGF method makes few assumptions, and it is validated by consistency with independent energy measurements and by the lack of systematic behavior in the residuals. In the four earthquake sequences we studied, we find that scaled energy does not vary systematically with earthquake size over the range $3 \leq M_w \leq 7.1$. Although we neglect particular site effects, such as directivity or small differences in focal mechanism, we average our energy estimates over many stations in each study area covering a wide range of azimuths.

[30] Our results support an earthquake model of self-similarity, also implying that other parameters, frictional energy, and rupture velocity do not vary strongly with earthquake size. The parametric scaling relations used to predict the level of high-frequency strong ground motion for potentially damaging earthquakes are largely based on measurements from earthquakes of a more modest size. In such estimates, self-similarity is assumed. If this were not the case, the strong ground motion for hypothetical larger events might currently be underestimated. Because constant scaled energy is consistent with constant stress drop, our results support the current practice of using constant stress drop for strong ground motion modeling, in that we do not find higher scaled energy in larger events.

[31] The strong dependence of E_R on size suggested by *Mayeda and Walter* [1996] and *Mayeda et al.* [2005] is not supported by our energy estimates. For each of the four study

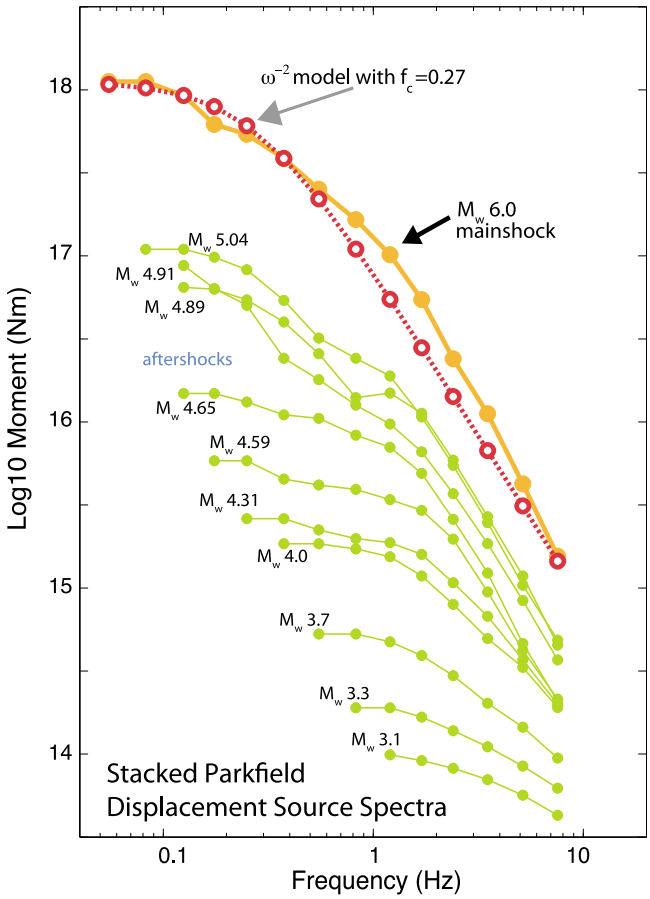

Figure 8. Stacked displacement (moment) source spectra for the Parkfield data. The M_w 6.0 mainshock is shown in heavy gray, and aftershocks are shown in lighter gray. All events are stacked over recordings at all stations used in the study. An idealized Brune ω^{-2} spectrum, with a corner frequency of 0.27 Hz, is shown with a black dashed line. The main event matches up well with the idealized spectrum.

areas, our best fit trend indicates a constant scaled energy, or an exponent of zero. Using our coda methodology outlined above, our results disagree with the results presented by Mayeda et al. (*Mayeda and Walter* [1996], *Mayeda et al.* [2003, 2005, and 2007], *Morasca et al.* [2005], and *Malagnini et al.* [2008]. They have consistently obtained a nonself-similar scaling between apparent stress and seismic moment, while we haven't. There are two important differences between their analysis and the one presented in this paper, namely, coda shape parameters and number of stations.

[32] First, *Mayeda et al.* [2003] estimated coda shape parameters and distance corrections using available stations in order to fit a synthetic coda envelope to the measured coda envelopes, as an intermediate step in their analysis. From the best fit envelopes, they estimated the amplitude spectra. We also used coda envelopes, which decayed over time; however, our coda spectral amplitude was a simple time-averaged value of the envelope. Because we used colocated events, we avoided the need to model the coda envelope decay parameters. By avoiding this middle step, and the adjustable parameters that it entailed, our method made fewer assumptions, rendering it more robust. Any disadvantage in our method due to shorter window lengths was more than compensated by the inclusion of up to 10 times as many stations in our analysis. As discussed above, we tested the reliability of our methodology by looking at effects of distance between source and receivers and the EGF assumptions made, and the results supported our assumptions.

[33] Second, in the results, *Mayeda et al.* [2003] have presented so far, only a few stations have been used (two to seven stations), compared to at least 23 stations used in our study. While using more stations provides a way for obtaining reliable uncertainty measurements, it does not explain the discrepancy in scaling. The possibility that coda shape parameters using a few stations could bias the results could be tested be using the method of Mayeda with more stations or comparing predicted envelopes with observed ones with stations not used in the fitting step. These tests, although very relevant to the resolving of the scaling of earthquakes, are beyond the scope of our paper.

[34] A second approach employed by *Mayeda et al.* [2007] created spectral ratios of the coda amplitude spectra to model the dependence of corner frequency on moment. Spectra were created, as in the work by *Mayeda et al.* [2003], but rather than making an EGF correction for the path, the spectral ratio was analyzed directly to determine the corner frequency and other source parameters. To determine the apparent stress, a reference event was used as a benchmark and scaled using the derived scaling parameter. The trade-off in fitting between moment, corner frequency, and the high-frequency decay rate may be highly sensitive, and the choice of reference apparent stress will affect the final apparent stress. We do not employ this method here, as it doesn't directly estimate radiated energy, and the corner frequency and spectral fall-off fitting trades off strongly and will be difficult with small events and band-limited recordings.

[35] While our results show that scaled energy is constant, this study is limited. Because of the EGF methodology, only events occurring in close proximity can be compared. The magnitude range is small, from $3 \leq M_w \leq 7.1$. M_W 3 is a lower limit due to noise, and M_W 7.1 is an upper limit on the size of earthquakes recorded in the western United States. Other studies using different methods have found constant scaled energy in smaller events, but it may not be accurate to compare studies. Thus, it is necessary to understand if this constant scaled energy is consistent in a single study over larger study areas with a wider range of magnitudes to truly understand earthquake source physics and strong ground motion.

[36] **Acknowledgments.** We thank Tom Hanks and Kevin Mayeda for helpful discussion. Comments from Rachel Abercrombie and Kevin Mayeda improved the manuscript. This research was supported by the Southern California Earthquake Center (SCEC) through the Extreme Ground Motion project group. SCEC is funded by NSF Cooperative Agreement EAR-0106924 and USGS Cooperative Agreement 02HQAG0008. The SCEC contribution number for this paper is 1287. Annemarie Baltay is supported by a Gabilan Stanford Graduate Fellowship. Data used in this analysis is from the CalTech, Anza, Berkeley, and TA networks, accessed through the IRIS Data Management Center and the SCEC Data Center.

References

Abercrombie, R. (1995), Earthquake source scaling relationships from −1 to 5 M_L using seismograms recorded at 2.5-km depth, *J. Geophys. Res.*, *100*(12), 24,015–24,036, doi:10.1029/95JB02397.

Aki, K. (1967), Scaling law of seismic spectrum, *J. Geophys. Res.*, *72*(4), 1217–1231, doi:10.1029/JZ072i004p01217.

Allmann, B. P., and P. M. Shearer (2009), Global variations of stress drop for moderate to large earthquakes, *J. Geophys. Res.*, *114*, B01310, doi:10.1029/2008JB005821.

Boatwright, J. (1978), Detailed spectral analysis of two small New York State earthquakes, *Bull. Seismol. Soc. Am.*, *68*, 1177–1131.

Boatwright, J., G. L. Choy, and L. C. Seekins (2002), Regional estimates of radiated seismic energy, *Bull. Seismol. Soc. Am.*, *92*, 1241–1255.

Brune, J. N. (1970), Tectonic stress and the spectra of seismic shear waves from earthquakes, *J. Geophys. Res.*, *75*(26), 4997–5009, doi:10.1029/JB075i026p04997.

Choy, G. L., and J. L. Boatwright (1995), Global patterns of radiated seismic energy and apparent stress, *J. Geophys. Res.*, *100*(B9), 18,205–18,228, doi:10.1029/95JB01969.

Hanks, T. C., and W. Thatcher (1972), A graphical representation of seismic source parameters, *J. Geophys. Res.*, *77*(23), 4393–4405, doi:10.1029/JB077i023p04393.

Hough, S. E. (1997), Empirical Green's function analysis: Taking the next step, *J. Geophys. Res.*, *102*(B3), 5369–5384, doi:10.1029/96JB03488.

Ide, S., and G. C. Beroza (2001), Does apparent stress vary with earthquake size?, *Geophys. Res. Lett.*, *28*(17), 3349–3352, doi:10.1029/2001GL013106.

Ide, S., G. C. Beroza, S. G. Prejean, and W. L. Ellsworth (2003), Apparent break in earthquake scaling due to path and site effects on deep borehole recordings, *J. Geophys. Res.*, *108*(B5), 2271, doi:10.1029/2001JB001617.

Imanishi, K., and W. Ellsworth (2006), Source scaling relationships of microearthquakes at Parkfield, CA, determined using the SAFOD pilot hole seismic array, in *Earthquakes: Radiated Energy and the Physics of Faulting*, *Geophys. Monogr. Ser.*, vol. 170, edited by R. Abercrombie et al., pp. 81–90, AGU, Washington, D. C.

Kanamori, H., and D. Anderson (1975), Theoretical basis of some empirical relations in seismology, *Bull. Seismol. Soc. Am.*, *65*, 1073–1095.

Kanamori, H., and L. Rivera (2004), Static and dynamic scaling relations for earthquakes and their implications for rupture speed and stress drop, *Bull. Seismol. Soc. Am.*, *94*, 314–319.

Kanamori, H., J. Mori, E. Hauksson, T. H. Heaton, L. K. Hutton, and L. M. Jones (1993), Determination of earthquake energy release and ML using TERRAscope, *Bull. Seismol. Soc. Am.*, *83*, 330–346.

Ma, S., S. Custodio, R. J. Archuleta, and P. Liu (2008), Dynamic modeling of the 2004 Mw 6.0 Parkfield, California, earthquake, *J. Geophys. Res.*, *113*, B02301, doi:10.1029/2007JB005216.

Malagnini, L., L. Scognamiglio, A. Mercuri, A. Akinci, and K. Mayeda (2008), Strong evidence for non-similar earthquake source scaling in central Italy, *Geophys. Res. Lett.*, *35*, L17303, doi:10.1029/2008GL034310.

Mayeda, K. (1993), Mb(LgCoda): A stable single station estimator of magnitude, *Bull. Seismol. Soc. Am.*, *83*, 851–861.

Mayeda, K., and W. R. Walter (1996), Moment, energy, stress drop, and source spectra of western United States earthquakes from regional coda

envelopes, *J. Geophys. Res.*, *101*(B5), 11,195–11,208, doi:10.1029/96JB00112.

Mayeda, K., A Hofstetter, J. L. O'Boyle, and W. R. Walter (2003), Stable and transportable regional magnitudes based on coda-derived moment rate spectra, *Bull. Seismol. Soc. Am.*, *93*, 224–239.

Mayeda, K., R. Gok, W. R. Walter, and A. Hofstetter (2005), Evidence for non-constant energy/moment scaling from coda-derived source spectra, *Geophys. Res. Lett.*, *32*, L10306, doi:10.1029/2005GL022405.

Mayeda, K., L. Malagnini, and W. R. Walter (2007), A new spectral ratio method using narrow band coda envelopes: Evidence for non-self-similarity in the Hector Mine sequence, *Geophys. Res. Lett.*, *34*, L11303, doi:10.1029/2007GL030041.

Morasca, P., K. Mayeda, L. Malagnini, and W. R. Walter (2005), Coda-derived source spectra, moment magnitudes and energy-moment scaling in the western Alps, *Geophys. J. Int.*, *160*, 263–275.

Mori, J., R. E. Abercrombie, and H. Kanamori (2003), Stress drops and radiated energies of aftershocks of the 1994 Northridge, California, earthquake, *J. Geophys. Res.*, *108*(B11), 2545, doi:10.1029/2001JB000474.

Mueller, C. S. (1985), Source pulse enhancement by deconvolution of an empirical Green's function, *Geophys. Res. Lett.*, *12*(1), 33–36, doi:10.1029/GL012i001p00033.

Pérez-Campos, X., and G. C. Beroza (2001), An apparent mechanism dependence of radiated seismic energy, *J. Geophys. Res.*, *106*, 11,127–11,136, doi:10.1029/2000JB900455

Prieto, G. A., P. M. Shearer, F. L. Vernon, and D. Kilb (2004), Earthquake source scaling and self-similarity estimation from stacking *P* and *S* spectra, *J. Geophys. Res.*, *109*, B08310, doi:10.1029/2004JB003084.

Shearer, P., G. A. Prieto, and E. Hauksson (2006), Comprehensive analysis of earthquake sournce spectra in southern California, *J. Geophys. Res.*, *111*, B06303, doi:10.1029/2005JB003979.

Singh, S. K., and M. Ordaz (1994), Seismic energy release in Mexican subduction zone earthquakes, *Bull. Seismol. Soc. Am.*, *84*, 1533–1550.

Takahashi, T., H. Sato, M. Ohtake, and K. Obara (2005), Scale dependence of apparent stress for earthquakes along the subducting Pacific plate in northeastern Honshu, Japan, *Bull. Seismol. Soc. Am.*, *95*, 1334–1345, doi:10.1785/0120040075.

Venkataraman, A., L. Rivera, and H. Kanamori (2002), Radiated energy from the 16 October 1999 Hector Mine earthquake: Regional and teleseismic estimates, *Bull. Seismol. Soc. Am.*, *92*, 1256–1265, doi:10.1785/0120000929.

Walter, W. R., K. M. Mayeda, R. Gok, and A. Hofstetter (2006), The scaling of seismic energy with moment: simple models compared with observations, in *Earthquakes: Radiated Energy and the Physics of Faulting*, *Geophys. Monogr. Ser.*, vol. 170, edited by R. Abercrombie et al., pp. 25–41, AGU, Washington, D. C.

Wyss, M. (1970), Stress estimates for South American shallow and deep earthquakes, *J. Geophys. Res.*, *75*(8), 1529–1544, doi:10.1029/JB075i008p01529.

Yamada, T., J. J. Mori, S. Ide, R. E. Abercrombie, H. Kawakata, M. Nakatani, Y. Iio, and H. Ogasawara (2007), Stress drops and radiated seismic energies of microearthquakes in a South African gold mine, *J. Geophys. Res.*, *112*, B03305, doi:10.1029/2006JB004553.

A. Baltay and G. C. Beroza, Department of Geophysics, Stanford University, Stanford, CA 94305, USA. (abaltay@stanford.edu)

G. Prieto, Physics Department, Universidad de los Andes, AA 4976, Bogotá, Colombia.